measure of the distortion. To do so we use the indices D_d and D_φ which are the percentage mean deviations of octahedron bond lengths and angles respectively from their mean values. They are given in Table 4 along with values calculated for $CaTiO_3$ ($n = \infty$). The mean distortions are fairly small, never greater than 1%. They are significantly greater in the CaO–TiO_2 compounds than in $Sr_3Ti_2O_7$ and there are no significant trends in the series $n = 2, 3, \infty$. However, the two types of octahedra in $n = 3$ structures appear to have a different degree of distortion especially with respect to angles (D_φ).

6. Concluding remarks

A procedure for predicting the space group of members of this series from the structure of the $n = \infty$ member is outlined in §3.1. and 3.2. It can be extended to indicate that the most likely space group for all n-even members is $Ccm2_1$ and for n-odd members is $Pcab$. This procedure should find general application in the solution of all such layered structures from known $n = \infty$ end members. Where our analysis has overlapped with that, for $n = 1$, of Aleksandrov (1987), the two approaches are in agreement.

The combined use of neutron powder diffraction and CBED in the solution of such structures is to be recommended. It should however, be noted that a space group could not be successfully allocated from the available CBED patterns without pattern simulations which relied on the neutron determined atomic positions.

Support under the National Research Fellowship scheme is gratefully acknowledged by EHK. Many thanks to Professor P. E. Fielding of the University of New England for preparation of the $Sr_3Ti_2O_7$ sample.

References

ALEKSANDROV, K. S. (1987). *Sov. Phys. Crystallogr.* **32**, 551–558.
DOLLASE, W. A. (1986). *J. Appl. Cryst.* **19**, 267–372.
DRY'S, M. & TRZEBIATOWSKI, W. (1957). *Rocz. Chem.* **31**, 489–496.
GLAZER, A. M. (1972). *Acta Cryst.* B**28**, 3384–3392.
GOODMAN, P., MATHESON, S. & WHITE, T. J. (1991). In preparation.
HAWKINS, K. D. & WHITE, T. J. (1991). In preparation.
HILL, R. J. & HOWARD, C. J. (1986). Australian Atomic Energy Commission Report No. M112. AAEC, Lucas Heights Research Laboratories, New South Wales, Australia.
HILL, R. J. & HOWARD, C. J. (1987). *J. Appl. Cryst.* **20**, 467–474.
HOWARD, C. J. (1982). *J. Appl. Cryst.* **15**, 615–620.
HOWARD, C. J., BALL, C. J., DAVIS, R. L. & ELCOMBE, M. M. (1983). *Aust. J. Phys.* **36**, 507–518.
KOOPMANS, H. J. A., VAN DE VELDE, G. M. H. & GELLINGS, P. J. (1983). *Acta Cryst.* C**39**, 1323–1325.
KWESTROO, W. & PAPING H. A. M. (1959). *J. Am. Ceram. Soc.* **42**, 293 299.
LUKASZEWICZ, K. (1959). *Rocz. Chem.* **33**, 239–242.
MEGAW, H. D. (1973). *Crystal Structures: A Working Approach.* Philadelphia: W. B. Saunders.
O'KEEFE, M. & HYDE, B. G. (1977). *Acta Cryst.* B**33**, 3802–3813.
ROTH, R. S. (1958). *J. Res. Natl Bur. Stand.* **61**, 437–440.
RUDDLESDEN, S. N. & POPPER, P. (1957). *Acta Cryst.* **10**, 538–539.
RUDDLESDEN, S. N. & POPPER, P. (1958). *Acta Cryst.* **11**, 54–55.
SEARS, V. J. (1984). Atomic Energy of Canada Ltd Report No. 8490. AECL, Chalk River, Canada.
SHIRANE, G. & YAMADA, Y. (1969). *Phys. Rev.* **177**, 858–863.
TILLOCA, G. & PEREZ Y JORBA, M. (1964). *Rev. Hautes Temp. Refract.* **1**, 331.
WILES, D. B. & YOUNG, R. A. (1981). *J. Appl. Cryst.* **14**, 149–151.

Acta Cryst. (1991). B**47**, 314–325

Determination of the Modulated Structure of the Inorganic Misfit Layer Compound $(PbS)_{1.18}TiS_2$

BY SANDER VAN SMAALEN, AUKE MEETSMA, GERRIT A. WIEGERS AND JAN L. DE BOER

Laboratory of Inorganic Chemistry, Materials Science Center, University of Groningen, Nijenborgh 16, *NL* 9747 *AG Groningen, The Netherlands*

(*Received* 15 *October* 1990; *accepted* 28 *November* 1990)

Abstract

Single-crystal X-ray diffraction results (Mo $K\bar{\alpha}$ radiation, $\lambda = 0.71073$ Å) are presented for the inorganic misfit layer compound titanium sulfide $(PbS)_{1.18}TiS_2$ which can be described as a two-component structure. The first subsystem (TiS_2, $\nu = 1$) has space-group symmetry $C2_1/m$, and a basic structure unit cell given by $a_{11} = 3.409$ (1), $a_{12} = 5.880$ (2), $a_{13} = 11.760$ (2) Å and $\alpha_1 = 95.29$ (2)°. The modulation wavevector is $\mathbf{q}^1 = \mathbf{a}^*_{21} = \alpha\mathbf{a}^*_{11}$, with $\alpha = 0.5878$ (3). Its subsystem superspace group is $P^{C2_1/m}_{1\ 1}$ (α, 0, 0). The second subsystem (PbS, $\nu = 2$) has space group $C2/m$ and a basic structure unit cell given by $a_{21} = 5.800$ (2), $a_{22} = 5.881$ (2), $a_{23} = 11.759$ (2) Å and $\alpha_2 = 95.27$ (2)°. The modulation wavevector is $\mathbf{q}^2 = \mathbf{a}^*_{11}$. The subsystem superspace group is $P^{C2/m}_{s\ 1}$ (α^{-1}, 0, 0). The relation between the

0108-7681/91/030314-12$03.00

two unit cells is defined by the common ($\mathbf{a}^*_{\nu 2}$, $\mathbf{a}^*_{\nu 3}$) plane. The symmetry of the complete system is described by the single superspace group $G_s = P^{C2/m}_s 1$ (α, 0, 0). Reciprocal lattice parameters for this superspace embedding are $\mathbf{a}^*_1 = \mathbf{a}^*_{11}$, $\mathbf{a}^*_2 = \mathbf{a}^*_{12}$, $\mathbf{a}^*_3 = \mathbf{a}^*_{13}$ and $\mathbf{a}^*_4 = \mathbf{a}^*_{21}$. Refinements on 1449 main reflections, with $I > 2{\cdot}5\sigma(I)$, converged smoothly to $R_{F^2} = 0{\cdot}064$ ($R_F = 0{\cdot}069$). The final structure model included displacive modulation parameters up to second harmonics for Pb and first harmonics for the other atoms. The largest modulation amplitudes are on both atoms of the PbS subsystem. They mainly desribe displacements parallel to the layers, along the commensurate direction $\mathbf{a}_{\nu 2}$. A detailed analysis is given of the coordination of the Pb ($\nu = 2$) and S ($\nu = 1$) atoms by plotting interatomic distances as a function of the fourth superspace coordinate.

Introduction

Inorganic misfit layer compounds are one example of the so-called intergrowth structures (Makovicky & Hyde, 1981; Wiegers, Meetsma, van Smaalen, Haange, Wulff, Zeinstra, de Boer, Kuypers, van Tendeloo, van Landuyt, Amelinckx, Meerschaut, Rabu & Rouxel, 1989). This type of crystal is characterized by the presence of two or more mutually incommensurate three-dimensional lattices. The structure is described by a finite fraction of the atoms being arranged periodically according to one lattice, while the remaining fraction has the periodicity of the second lattice. Intergrowth structures form a class of incommensurate phases which is essentially different from either modulated structures or quasicrystals.

The structures of the misfit layer compounds are characterized by an alternate stacking of TS_2 and MS layers (both M and T represent a metal atom) (Makovicky & Hyde, 1981; Wiegers *et al.*, 1989). The TS_2 layers form the first subsystem ($\nu = 1$) with periodicity according to the lattice $\Lambda_1 = \{\mathbf{a}_{11}, \mathbf{a}_{12}, \mathbf{a}_{13}\}$. The second subsystem ($\nu = 2$) is formed by the MS layers with periodicity according to $\Lambda_2 = \{\mathbf{a}_{21}, \mathbf{a}_{22}, \mathbf{a}_{23}\}$. For T = Nb or Ta [*e.g.* $(SnS)_{1{\cdot}17}NbS_2$] both subsystems have an orthorhombic lattice, with the c axis perpendicular to the layers (Meetsma, Wiegers, Haange & de Boer, 1989; van Smaalen, 1989). Depending on the combination *CC*, *FF* or *CF* for the *C*- or *F*-centring of either cell, we have $\mathbf{a}_{23} = \mathbf{a}_{13}$ or $\mathbf{a}_{23} = \frac{1}{2}\mathbf{a}_{13}$. The unit-cell setting used previously for many examples had $\mathbf{a}_{12} = \mathbf{a}_{22}$ but $\mathbf{a}_{11}$ was only parallel to $\mathbf{a}_{21}$. Their incommensurate length ratio defines the incommensurability in these orthorhombic inorganic misfit layer compounds.

In a recent paper it was argued that when the NbS_2 or TaS_2 slab is replaced by a TS_2 slab with T octahedrally coordinated, a monoclinic symmetry results (Wiegers, Meetsma, van Smaalen, Haange & de Boer, 1990). The angle between $\mathbf{a}_{\nu 2}$ and $\mathbf{a}_{\nu 3}$ is then greater than 90°, with $\cos(\alpha_\nu) = -a_{\nu 2}/(6a_{\nu 3})$. Misfit layer compounds with monoclinic sublattices are observed for $(PbS)_{1{\cdot}13}VS_2$ and $(PbS)_{1{\cdot}18}TiS_2$ (Gotoh, Goto, Kawaguchi, Oosawa & Onoda, 1990; Onoda, Kato, Gotoh & Oosawa, 1990; Wiegers, Meetsma, van Smaalen *et al.*, 1990).

The structure of intergrowth compounds can be described by the so-called superspace groups (Janner & Janssen, 1980). For the orthorhombic misfit layer compound $(SnS)_{1{\cdot}17}NbS_2$ this has been done previously (van Smaalen, 1989). The first result, which is more of philosophical importance, is that the superspace-group approach shows that intergrowth compounds indeed have space-group symmetry. For the basic structure, its principal result was to define a relation between the space groups of the individual subsystems. This allowed the determination of the proper non-centrosymmetric space group for the SnS subsystem (van Smaalen, 1989). Subsequently, this principle was applied to other misfit compounds (Wiegers *et al.*, 1989). The symmetry restrictions for the modulation functions were also given, but values for the remaining independent parameters were not determined. Recently, refinements of the modulated structures of $(LaS)_{1{\cdot}20}CrS_2$ and $(PbS)_{1{\cdot}12}VS_2$ were published (Kato, 1990; Onoda *et al.*, 1990).

In this paper the complete superspace-group description for $(PbS)_{1{\cdot}18}TiS_2$ will be given, including a determination of the modulation parameters. Refinements were performed with the computer program *COMPREF* (Petříček, Maly, Coppens, Bu, Cisarova & Frost-Jensen, 1991), which is the extension for intergrowth structures of the refinement program *JANA* for modulated structures (Petříček & Coppens, 1988). The coordination of the various atoms is analyzed by plotting interatomic distances as a function of the fourth superspace coordinate, both with respect to atoms in the same subsystem and with respect to the atoms of the other subsystem.

Experimental

A powder sample was prepared from the elements; the ratio of the elements was chosen such as to correspond with the expected ratio in view of a_{11} and a_{21} from the PbS double layer in $(PbS)_{1{\cdot}14}NbS_2$ (Wiegers, Meetsma, Haange, van Smaalen, de Boer, Meerschaut, Rabu & Rouxel, 1990) and 1*T*-TiS_2 (Chianelli, Scanlon & Thompson, 1975) respectively. The mixture of elements was heated at 1073 K in an evacuated quartz tube for seven days. Crystals suitable for electrical transport measurements and single-crystal X-ray diffraction were obtained by vapour transport using chlorine, for which about 1% by weight of $(NH_4)_2PbCl_6$ was used. Crystals grew as

thin platelets at the cold part of the gradient between 993–923 K.

Single-crystal X-ray diffraction was performed on an Enraf–Nonius CAD-4F diffractometer using monochromatized Mo $K\bar{\alpha}$ radiation ($\lambda = 0.71073$ Å) with a crystal of approximate dimensions $0.18 \times 0.22 \times 0.008$ mm^3. All reflections could be indexed on two mutually incommensurate monoclinic unit cells. For comparison with the orthorhombic misfit layer compounds *C*-centred cells were used. Unit-cell dimensions and their standard deviations were determined independently for each subsystem from the setting angles of 22 reflections in the range $22.26 < \theta < 27.50°$ in four alternative settings (de Boer & Duisenberg, 1984).

For TiS_2 (first subsystem, $\nu = 1$), the lattice parameters were $a_{11} = 3.409$ (1), $a_{12} = 5.880$ (2), $a_{13} = 11.760$ (2) Å, $\alpha_1 = 95.29$ (2)° and $V = 234.7$ (1) Å^3. For the PbS subsystem ($\nu = 2$), the lattice parameters were $a_{21} = 5.800$ (2), $a_{22} = 5.881$ (1), $a_{13} = 11.759$ (2) Å, $\alpha_1 = 95.27$ (2)° and $V = 399.4$ (2) Å^3. The results showed that both $a_{\nu 2}$, both $a_{\nu 3}$ and both α_ν differed by less than their standard deviations. Analysis of the diffraction pattern did not show any splitting of the common (0, *k*, *l*) reflections. As is theoretically expected, and is also found for the orthorhombic misfit compounds, this implied $\mathbf{a}_{12} = \mathbf{a}_{22}$ and $\mathbf{a}_{13} = \mathbf{a}_{23}$, while the $\mathbf{a}_{\nu 1}$ axes, being parallel, had an incommensurate length ratio $a_{11}/a_{21} = \alpha$. Therefore, the average values of the lattice parameters were used to describe the structure. They are $a_2 = \frac{1}{2}(a_{12} + a_{22}) = 5.881$ (1), $a_3 = \frac{1}{2}(a_{13} + a_{23}) = 11.760$ (2) and $\alpha = \frac{1}{2}(\alpha_1 + \alpha_2) = 95.28$ (2)°. The *a* axes for the two subsystems were found to be $a_{11} = 3.409$ (1) and $a_{21} = 5.800$ (2) Å, respectively. From these the incommensurate ratio was determined as $\alpha = 0.5878$ (3).

The data collection was performed separately for the subsystems. Reflection intensities were measured at the nodes of the reciprocal lattices of the respective subsystems. All main reflections were measured in one hemisphere up to $\theta = 35°$ for TiS_2. Intensities for PbS were measured up to $\theta = 45°$ because of the presence of a stronger scatterer. The experimental stability was checked by three standard reflections measured every 2 h of X-ray exposure time; they showed a long-term variation of less than 1%. The intensities were corrected for the scale variation, Lorentz and polarization effects, and for absorption using a Gaussian integration method (grid: $10 \times 10 \times 6$; Spek, 1982). Further details of the data collection are given in Table 1.

For TiS_2, 1122 measured reflections were combined into 593 unique reflections, using Laue symmetry 2/*m*. The internal consistency was $R_I = (\sum|I_i - I_i^{Av}|)/(\sum I_i) = 0.064$. For PbS, the same Laue symmetry reduced 3494 measured intensities to 1755 unique reflections, with $R_I = 0.042$. The method of measurement means that the (0, *k*, *l*) reflections were measured twice. Each data set contains intensities for the same (0, *k*, *l*) reflections, measured on the same crystal. These reflections were used to bring the two data sets onto a common scale. For 121 reflections present in both data sets, this resulted in a scale factor of 1.233 (3) which was used to multiply the PbS intensities. The internal consistency was found to be $R_I = 0.011$. The result was a single data set for the misfit compound with 2227 unique reflections. Refinements were performed on reflections with $I > 2.5\sigma(I)$. With this criterion for observability, the number of unique reflections reduced to 1449 [165 (0, *k*, *l*) reflections, 331 for the TiS_2 subsystem and 953 for PbS].

Satellite reflections were not observed on Weissenberg photographs made with Cu $K\alpha$ radiation. In addition, a random scan for reflections on the diffractometer did not reveal any satellites. Therefore, only main reflections were included in the present analysis.

Table 1. *Data-collection parameters*

	PbS part	TiS_2 part
Diffractometer	Enraf–Nonius CAD-4F	
Radiation	Mo $K\bar{\alpha}$, $\lambda = 0.71073$ Å	
Monochromator	Graphite	
Temperature (K)	295	
θ range, min., max. (°)	1.74, 45.0	1.74, 35.0
$\omega/2\theta$ scan (°)	$\Delta\omega = 0.90 + 0.35\tan\theta$	$\Delta\omega = 0.90 + 0.35\tan\theta$
Range of (h,k,l)	h −11→11, k 0→11, l −23→23	h −5→5, k 0→9, l −18→18
Crystal to receiving aperture distance (mm)	173	
Horizontal, vertical aperture (mm)	4.0, 4.5	
Reference reflections; r.m.s. deviation (%)	220; 0.40 $\bar{2}22$; 0.36 203; 0.37	005; 1.40 00$\bar{2}$; 0.60
Drift correction	0.948–1.000	0.996–1.000
Min. and max. absorption correction factor	1.89–29.49	1.89–42.72
X-ray exposure time (h)	61.4	18.0
Total data	3494	1122
Unique data	1755	593

Superspace-group symmetry

Superspace-group analysis of intergrowth crystals was introduced by Janner & Janssen (1980), and was further developed by van Smaalen (1991*a*). Its application to the orthorhombic inorganic misfit layer compounds $(SnS)_{1.17}NbS_2$ and $(LaS)_{1.14}NbS_2$ has been reported previously (van Smaalen, 1989, 1991*b*; Wiegers, Meetsma, Haange *et al.*, 1990). The description for the monoclinic compound studied here is only slightly different and will therefore be given without much detail.

The starting point of the superspace-group approach is the description of the diffraction pattern by a finite set of integer indices. The common (**b***c**) plane implies that four reciprocal vectors are

sufficient to obtain an integer indexing of the complete diffraction pattern. This set, $M = \{\mathbf{a}_1^*,...,\mathbf{a}_4^*\}$, can be defined as $\mathbf{a}_1^* = \mathbf{a}_{11}^*$, $\mathbf{a}_2^* = \mathbf{a}_{12}^*$, $\mathbf{a}_3^* = \mathbf{a}_{13}^*$ and $\mathbf{a}_4^* = \mathbf{a}_{21}^*$. The $\mathbf{a}_{\nu i}^*$ ($\nu = 1, 2$; $i = 1, 2, 3$) are the reciprocal lattice vectors of the subsystem unit cells as defined in the *Experimental* section. Superspace was obtained in the usual way, by identification of the four basis vectors of M with the perpendicular projection of four independent translation vectors in a $(3+1)$-dimensional space (Janner & Janssen, 1980; de Wolff, Janssen & Janner, 1981).

The basis vectors of the subsystem reciprocal lattices, Λ_ν^*, can now be written as an integral linear combination of the basis vectors in M (Janner & Janssen, 1980):

$$\mathbf{a}_{\nu i}^* = \sum_{k=1}^{4} Z_{ik}^{\nu} \mathbf{a}_k^*, \quad i = 1,2,3. \tag{1}$$

The corresponding axes $\mathbf{a}_{\nu i}^*$ are parallel, so the matrix defining the components of the fourth reciprocal vector in M with respect to the first three, is given by,

$$\sigma = (\alpha, 0, 0). \tag{2}$$

The interaction between the subsystems implies that each one will be modulated, with a modulation wavevector given by the periodicities of the reciprocal lattice of the other subsystem. The modulation wavevectors, $\mathbf{q}^\nu$, can be obtained from the vectors in M, by application of an integer matrix V^ν, defined such that:

$$\mathbf{q}^\nu = \sum_{k=1}^{4} V_{1k}^{\nu} \mathbf{a}_k^*. \tag{3}$$

Juxtaposition of the $3 \times (3+1)$ matrix Z^ν and the $1 \times (3+1)$ matrix V^ν defines a $(3+1) \times (3+1)$ matrix W^ν as (van Smaalen, 1991*a*):

$$W^\nu = \begin{pmatrix} Z^\nu \\ V^\nu \end{pmatrix}. \tag{4}$$

The requirements for V^ν are that: (i) W^ν is non-singular and (ii) the entire diffraction pattern can be described. For the present analysis the following matrices were used:

$$W^1 = \begin{bmatrix} 1 & 0 & 0 & 0 \\ 0 & 1 & 0 & 0 \\ 0 & 0 & 1 & 0 \\ 0 & 0 & 0 & 1 \end{bmatrix}, \quad W^2 = \begin{bmatrix} 0 & 0 & 0 & 1 \\ 0 & 1 & 0 & 0 \\ 0 & 0 & 1 & 0 \\ 1 & 0 & 0 & 0 \end{bmatrix}. \tag{5}$$

It is not difficult to show that any main reflection or satellite of subsystem ν, with indices $(h_\nu, k_\nu, l_\nu, m_\nu)$ with respect to Λ_ν^* and the vector $\mathbf{q}^\nu$, has integer indices with respect to M, given by:

$$(H, K, L, M) = (h_\nu, k_\nu, l_\nu, m_\nu) W^\nu. \tag{6}$$

Table 2. *Elements of the superspace group G_s, together with the corresponding elements of both subsystem superspace groups G_s^ν, $\nu = 1, 2$*

n_i, $i = 1,...,4$ assumes all integer values. All elements may be combined with the centring translation and/or any lattice translation. The position of the origin relative to the symmetry elements is given by the values of τ_i, $i = 1,...,4$. In this paper, $\tau_i = 0$ is used.

$G_s = G_s^1$	G_s^2
$(E\ 1\|n_1, n_2, n_3, n_4)$	$(E\ 1\|n_4, n_2, n_3, n_4)$
$(E\ 1\|\frac{1}{2}, \frac{1}{2}, 0, \frac{1}{2})$	$(E\ 1\|\frac{1}{2}, \frac{1}{2}, 0, \frac{1}{2})$
$(i\ \bar{1}\|\tau_1, \tau_2, \tau_3, \tau_4)$	$(i\ \bar{1}\|\tau_4, \tau_2, \tau_3, \tau_1)$
$(m_x\ \bar{1}\|\tau_1, 0, 0, \frac{1}{2} + \tau_4)$	$(m_x\ \bar{1}\|\frac{1}{2} + \tau_4, 0, 0, \tau_1)$
$(2_x\ 1\|0, \tau_2, \tau_3, \frac{1}{2})$	$(2_x\ 1\|\frac{1}{2}, \tau_2, \tau_3, 0)$

With (6) and the W^ν matrices from (5), the four-integer indexing of the reflections for both subsystems can be calculated. The first subsystem gives rise to $(H, K, L, 0)$ reflections and the second subsystem gives $(0, K, L, M)$ reflections. As no intensity could be found at the satellite positions, all (H, K, L, M) reflections with both H and M not equal to zero are absent.

Considering the superspace indexing, the diffraction pattern again has monoclinic symmetry, now generated by $(2_x\ 1)$ and $(m_x\ \bar{1})$. Systematic extinctions were found to be $H + K + M =$ odd is absent for the (H, K, L, M) reflections. This implies a C-centring given by the centring translation,

$$(\tfrac{1}{2}, \tfrac{1}{2}, 0, \tfrac{1}{2}). \tag{7}$$

Thus, the $(3+1)$-dimensional Bravais class is $P_{\bar{1}}^{C2/m}$ $(\alpha, 0, 0)$, with C a tentative symbol representing the centring translation (7). In the standard setting this corresponds to the Bravais class given by the same symbol, but with C representing $(\frac{1}{2}, \frac{1}{2}, 0, 0)$ (de Wolff *et al.*, 1981).

No further extinction conditions were observed. However, it was noted that the condition given above reduces to $H + M =$ odd is absent for the $(H, 0, 0, M)$ reflections. As no satellites were measured, this implies the condition $H =$ odd is absent and $M =$ odd is absent for these reflections. This latter condition indicates the presence of the symmetry elements $(2_x\ 1|\frac{1}{2}, 0, 0, 0)$ and $(2_x\ 1|0, 0, 0, \frac{1}{2})$ in the superspace group describing the structure. The former condition suggested the symmetry elements $(2_x\ 1|0, 0, 0, 0)$ and $(2_x\ 1|\frac{1}{2}, 0, 0, \frac{1}{2})$. Therefore, for a centrosymmetric structure, there are two possible superspace groups compatible with the Laue symmetry and extinction conditions: $G_s(\mathrm{I}) = P_{s\,\bar{1}}^{C2/m}$ $(\alpha, 0, 0)$ and $G_s(\mathrm{II}) = P_{\bar{1}}^{C2/m}$ $(\alpha, 0, 0)$. Note that $G_s(\mathrm{I})$ is equivalent to $P_{\bar{1}}^{C2_1/m}$ $(\alpha, 0, 0)$, while $G_s(\mathrm{II})$ is equivalent to $P_{s\,\bar{1}}^{C2_1/m}$ $(\alpha, 0, 0)$. For a non-centrosymmetric structure, the corresponding non-centrosymmetric superspace groups should be used, *e.g.* $G_s'(\mathrm{I}) = P_s^{C2}$ $(\alpha, 0, 0)$, *etc.*

Table 3. *Structure coordinates and temperature parameters* (Å^2) *as obtained from refinement of the basic structure*

Coordinates refer to the subsystem lattice basis. Standard deviations in the last digits are given in parentheses. When these are not given, the corresponding parameters are fixed by symmetry. The temperature factor which appears in the expression for the structure factor is defined by $T = \exp[-(\beta_{11}h_{\nu 1}h_{\nu 1} + \beta_{22}h_{\nu 2}h_{\nu 2} + \beta_{33}h_{\nu 3}h_{\nu 3} + 2\beta_{23}h_{\nu 2}h_{\nu 3})]$ and $\beta_{ij} = 2\pi^2 U_{ij} a^*_{\nu i} a^*_{\nu j}$. For all atoms, U_{12} and U_{13} are zero as a consequence of the symmetry.

	ν	$x^0_{\nu 1}$	$x^0_{\nu 2}$	$x^0_{\nu 3}$	U_{11}	U_{22}	U_{33}	U_{23}
Ti	1	0·0	0·0	0·0	0·0133 (8)	0·0107 (6)	0·0142 (7)	0·0015 (5)
Si	1	0·5	0·1888 (3)	0·1221 (2)	0·0096 (7)	0·0094 (5)	0·0110 (6)	0·0028 (5)
Pb	2	0·25	0·0256 (1)	0·63638 (5)	0·0459 (3)	0·0338 (3)	0·0223 (2)	0·0033 (2)
S2	2	0·75	0·0184 (6)	0·5989 (2)	0·0499 (23)	0·0239 (13)	0·0209 (12)	0·0019 (10)

Analysis of the satellite intensities would make it possible to distinguish between the two extinction conditions, and thus directly determine whether the superspace group is G_s(I) or G_s(II). Obviously, the complete structure determination is needed to decide on the presence of the inversion centre. In the present study, refinements have shown the correct superspace group to be $G_s(\mathrm{I}) = G_s = P^{C2/m}_{s\,1}(\alpha, 0, 0)$.

The matrices W^ν [equation (5)] define the coordinate transformation between superspace and the subsystem superspace embedding. The elements $(R^\nu_s|\tau^\nu_s)$ of the subsystem superspace group are obtained as (van Smaalen, 1991*a*,*b*):

$$R^\nu_s = W^\nu R_s (W^\nu)^{-1} \qquad (8a)$$

$$\tau^\nu_s = W^\nu \tau_s. \qquad (8b)$$

Thus for the subsystem superspace groups $G^1_s = G_s$ and $G^2_s = P^{C2_1/m}_{1\,\bar{1}}(\alpha^{-1}, 0, 0)$ were obtained, with C again defined by (7). The elements of both groups G_s and G^2_s are given in Table 2. Similarly, the space groups describing the symmetry of the basic structure of each subsystem can be obtained as the restriction of G^ν_s to three-dimensional space. Thus, we have $G_1 = C2/m$ and $G_2 = C2_1/m$. Note that, unlike the subsystem superspace groups, G_1 and G_2 are equivalent. The different notation reflects that one particular possibility was chosen for combining the inversion centres of the subsystems.

Determination of the basic structure

A trial model for the structure of the PbS subsystem was deduced from the geometry of the PbS double layer in $(PbS)_{1.14}NbS_2$ (Wiegers, Meetsma, Haange *et al.*, 1990). The starting coordinates of S1 were from a model with Ti in trigonal antiprismatic coordination. The PbS subsystem was centred at $x_{23} = 0.5$ and the TiS_2 layer was centred at $x_{13} = 0$. As mentioned in the previous section, there are two possible superspace groups for describing the symmetry. They correspond to the two possible ways in which the inversion centres of the two subsystems can be aligned. The two trial structures thus obtained give rise to different intensities for the (0, K, L, 0) reflections. Therefore, they can be discriminated on the basis of a structure-factor calculation.

Refinement on F^2 for the model according to G_s(II) resulted in a fit with $R_{F^2} = 0.39$. Refinement of the structural parameters in the model according to G_s(I) gave $R_{F^2} = 0.072$. This shows the latter symmetry to be the correct choice. All calculations were performed with the computer program *COMPREF* (Petříček *et al.*, 1991).

The partial R factors for the final fit in G_s show a rather high value for the reflection set of the TiS_2 subsystem. This is also found in, for example, $(LaS)_{1.20}CrS_2$ (Kato, 1990). The explanation is based on the influence of the modulation on the reflection intensities (see next section). The atomic coordinates and temperature factors for the basic structure are given in Table 3. They show that both atoms, Pb and S2, of the PbS subsystem as well as S1 of the TiS_2 subsystem are on the mirror plane, whereas Ti is on the inversion centre.

From the size of the subsystem unit cells and the number of formula units per cell ($Z = 4$ for PbS and $Z = 2$ for TiS_2), the composition of the compound is calculated as $(PbS)_{1.18}TiS_2$ [*viz.* $1.18 = 2 \times (3.409/5.800)$].

Refinement of the modulated structure

As explained elsewhere (van Smaalen, 1991*b*), the basic structure coordinates for each subsystem with respect to its own subsystem basis, are given by:

$$\bar{x}_{\nu i}(j) = n_{\nu i} + x^0_{\nu i}(j) - (Z^\nu_d t)_i \qquad (9)$$

where $n_{\nu i}$ are integers describing the unit cell and $x^0_{\nu i}(j)$ are the coordinates of atom j within one unit cell, which correspond to those given in Table 3. The matrix Z^ν_d is defined by writing Z^ν as the juxtaposition of a 3×3 matrix Z^ν_3 and a $3 \times d$ matrix Z^ν_d ($d = 1$): $Z^\nu = (Z^\nu_3 Z^\nu_d)$. The t-dependent part reflects a shift of the origin with respect to that obtained with the standard superspace description for subsystem ν. This term is necessary to retain the relative phase between the subsystems, when varying the physical space section $\mathbb{E}^3(t)$.

The atomic positions in the modulated structure are the sum of $\bar{x}_{\nu i}$ and the modulation function:

$$x_{\nu i}(j) = \bar{x}_{\nu i}(j) + u^j_{\nu i}(\bar{x}_{\nu s4}) \qquad (10)$$

where $\bar{x}_{\nu i}(j)$ is defined in (9); $u^j_{\nu i}(\bar{x}_{\nu s4})$ is the modulation function of atom j, which is periodic with periodicity 1 in its argument. $\bar{x}_{\nu s4}$ is the fourth superspace coordinate for the basic structure, in the subsystem superspace embedding. It is given by (van Smaalen, 1991*b*),

$$\bar{x}_{\nu s4} = \sigma_\nu . \bar{\mathbf{x}}_\nu + V^\nu_d t \tag{11}$$

where $V^\nu = (V^\nu_3 V^\nu_d)$, similar to the decomposition of Z^ν. For each subsystem, the subsystem σ matrix represented the coordinates of the modulation wavevector $\mathbf{q}^\nu$. For $(PbS)_{1.18}TiS_2$, the following relationships were obtained,

$$\sigma_1 = (\alpha, 0, 0)$$
$$\sigma_2 = (\alpha^{-1}, 0, 0). \tag{12}$$

The t-dependent part in (11) and the t-dependence in $\bar{x}_{\nu i}(j)$, together define the relation between the phases of the modulation functions in the two subsystems, and the relative position of the subsystem lattices along the incommensurate direction.

The subsystem superspace embedding is obtained from (9)–(12) in the usual way (de Wolff *et al.*, 1981; van Smaalen, 1991*b*). The one-dimensional point set comprising the atom in the common superspace is obtained as,

$$\begin{pmatrix} x_{s1} \\ x_{s2} \\ x_{s3} \\ x_{s4} \end{pmatrix} = \begin{pmatrix} \bar{x}_{s1} \\ \bar{x}_{s2} \\ \bar{x}_{s3} \\ \bar{x}_{s4} \end{pmatrix} + Y^\nu \begin{pmatrix} u_{\nu 1}(\bar{x}_{\nu s4}) \\ u_{\nu 2}(\bar{x}_{\nu s4}) \\ u_{\nu 3}(\bar{x}_{\nu s4}) \end{pmatrix} \tag{13}$$

with the corresponding basic structure position:

$$\begin{pmatrix} \bar{x}_{s1} \\ \bar{x}_{s2} \\ \bar{x}_{s3} \\ \bar{x}_{s4} \end{pmatrix} = Y^\nu \begin{pmatrix} \bar{x}_{\nu 1} \\ \bar{x}_{\nu 2} \\ \bar{x}_{\nu 3} \end{pmatrix} + \begin{pmatrix} 0 \\ 0 \\ 0 \\ t \end{pmatrix}. \tag{14}$$

The fourth coordinate of the subsystem superspace description, $\bar{x}_{\nu s4}$, follows from (11). It can be written as a function of the four $\bar{x}_{sk}$. Y^ν is the pseudo-inverse of Z^ν, suitable for the embedding defined by (1)–(6) (van Smaalen, 1989, 1991*a*):

$$Y^1 = \begin{bmatrix} 1 & 0 & 0 \\ 0 & 1 & 0 \\ 0 & 0 & 1 \\ \alpha & 0 & 0 \end{bmatrix}, \qquad Y^2 = \begin{bmatrix} \alpha^{-1} & 0 & 0 \\ 0 & 1 & 0 \\ 0 & 0 & 1 \\ 1 & 0 & 0 \end{bmatrix}. \tag{15}$$

The coordinates given in (9) and (10) are with respect to the subsystem lattice basis. The effect of the symmetry operators of G_s is then obtained by application of the subsystem superspace group matrix representations $(R^\nu_s|\tau^\nu_s)$ to these coordinates (van Smaalen, 1991*b*):

$$\begin{pmatrix} x'_{\nu 1} \\ x'_{\nu 2} \\ x'_{\nu 3} \end{pmatrix} = R^\nu_3 \begin{pmatrix} \bar{x}_{\nu 1} \\ \bar{x}_{\nu 2} \\ \bar{x}_{\nu 3} \end{pmatrix} + \begin{pmatrix} \tau^\nu_1 \\ \tau^\nu_2 \\ \tau^\nu_3 \end{pmatrix} + (R^\nu_3 Z^\nu_d - Z^\nu_d)t + R^\nu_3 \begin{pmatrix} u_{\nu 1}[(R^\nu_d)^{-1}(\bar{x}'_{\nu s4} - \tau^\nu_4)] \\ u_{\nu 2}[(R^\nu_d)^{-1}(\bar{x}'_{\nu s4} - \tau^\nu_4)] \\ u_{\nu 3}[(R^\nu_d)^{-1}(\bar{x}'_{\nu s4} - \tau^\nu_4)] \end{pmatrix}. \tag{16}$$

The term $(R^\nu_d Z^\nu_d - Z^\nu_d)t$ explicity accounts for the effect of the origin shift $Z^\nu_d t$ on the translational part of the symmetry operator.

Symmetry restrictions on the basic structure coordinates and the modulation functions can be obtained when the symmetry operator maps the point set representing one atom onto itself:

$$\begin{pmatrix} x'_{\nu 1}(t) \\ x'_{\nu 2}(t) \\ x'_{\nu 3}(t) \end{pmatrix} = \begin{pmatrix} x_{\nu 1}(t') \\ x_{\nu 2}(t') \\ x_{\nu 3}(t') \end{pmatrix}. \tag{17}$$

Note that t and t' need not be the same. Substitution of (9) and (10) into (17), and use of (16) gives for the basic structure coordinates,

$$\begin{pmatrix} n_{\nu 1} + x^0_{\nu 1} \\ n_{\nu 2} + x^0_{\nu 2} \\ n_{\nu 3} + x^0_{\nu 3} \end{pmatrix} = R^\nu_3 \begin{pmatrix} n_{\nu 1} + x^0_{\nu 1} \\ n_{\nu 2} + x^0_{\nu 2} \\ n_{\nu 3} + x^0_{\nu 3} \end{pmatrix} + \begin{pmatrix} \tau^\nu_1 \\ \tau^\nu_2 \\ \tau^\nu_3 \end{pmatrix}. \tag{18}$$

Restrictions on the modulation functions can be obtained from

$$\begin{pmatrix} u_{\nu 1}(\bar{x}_{\nu s4}) \\ u_{\nu 2}(\bar{x}_{\nu s4}) \\ u_{\nu 3}(\bar{x}_{\nu s4}) \end{pmatrix} = R^\nu_3 \begin{pmatrix} u_{\nu 1}[(R^\nu_d)^{-1}(\bar{x}_{\nu s4} - \tau^\nu_4)] \\ u_{\nu 2}[(R^\nu_d)^{-1}(\bar{x}_{\nu s4} - \tau^\nu_4)] \\ u_{\nu 3}[(R^\nu_d)^{-1}(\bar{x}_{\nu s4} - \tau^\nu_4)] \end{pmatrix}. \tag{19}$$

Restrictions for the basis structure coordinates are the same as determined in the previous section (Table 3). To derive the corresponding restrictions on the modulation functions, they are written as a Fourier series:

$$u^j_{\nu i}(\bar{x}_{\nu s4}) = \sum_{n=1}^{\infty} A^j_{ni} \sin(2\pi n \bar{x}_{\nu s4}) + B^j_{ni} \cos(2\pi n \bar{x}_{\nu s4}) \tag{20}$$

for j = Ti, S1, Pb and S2, respectively. $\bar{x}_{\nu s4}$ is given in (11). Substitution of (12) gives a different expression for the two subsystems:

$$\bar{x}_{1s4} = \alpha[n_{11} + x^0_{11}(j)] + t \tag{21a}$$

$$\bar{x}_{2s4} = \alpha^{-1}[n_{21} + x^0_{21}(j) - t]. \tag{21b}$$

Non-zero $x^0_{\nu 1}$ can be obtained for atoms shifted by the centring translation. The restrictions on the Fourier components are obtained from (19) and are given in Table 4. They apply to the atoms on special positions as defined in Table 3.

Table 4. *Symmetry restrictions on the modulation functions*

The restrictions applying to harmonic amplitudes are similar to those defined in (20), but with the argument $\bar{x}_{\nu,4}$ replaced by $(\bar{x}_{1,4} - \frac{1}{2}\tau_4)$ for $\nu = 1$ and by $(\bar{x}_{2,4} - \frac{1}{2}\tau_4)$ for $\nu = 2$. The coordinates are relative to Λ_ν for each subsystem, $\nu = 1, 2$. The parameters $\bar{x}_{\nu,4}$ ($\nu = 1, 2$) are defined in (11) and (21).

		Coordinate	Odd harmonics	Even harmonics
Ti	($\nu = 1$)	u_{11}	Zero	Odd
		u_{12}	Odd	Zero
		u_{13}	Odd	Zero
S1	($\nu = 1$)	u_{11}	Even	Odd
		u_{12}	Odd	Even
		u_{13}	Odd	Even
Pb	($\nu = 2$)	u_{21}	Odd	Odd
		u_{22}	Even	Even
		u_{23}	Even	Even
S2	($\nu = 2$)	u_{21}	Odd	Odd
		u_{22}	Even	Even
		u_{23}	Even	Even

To determine the modulation, the first harmonics for Pb (three parameters) were added to the list of independent parameters. Refinement against the complete data set (which includes only main reflections) resulted in an improvement of the R_{F^2} value from 0·072 to 0·065. Inspection of the reflection list shows the largest effect to be an improvement of the fit of the (1, K, L, 0) reflections. The reason is that these reflections are main reflections of the TiS_2 subsystem, but at the same time they are also first-order satellites of the second subsystem. As the latter is modulated now, the contribution of PbS to these reflections is obtained far more accurately. On the other hand, the effect of the modulation on the PbS main reflections is compensated by a change of the temperature factors. This is also seen in the partial R factor, which for the main reflections of the TiS_2 subsystem is lowered from 0·137 to 0·099. Subsequent introduction of the first harmonics for all four atoms, and of the second-harmonic modulation for Pb gave a further lowering of the R factor. More additional harmonics led to a singular matrix, and thus could not be refined.

The parameters for the final structure model are given in Table 6 (basic structure parameters) and Table 7 (modulation function amplitudes). The R factors for the final structure model are given in Table 5.*

The R-factor values for the best structure model (*Table 5*), show that a reasonably good fit was obtained. Analysis of the reflection list shows that the largest ΔF values occur for the $h_1 = 3$ reflections of the TiS_2 subsystem and the $h_2 = 5$ reflections of the PbS subsystem. This can be explained as a result of the nearly commensurate value of $a_{\nu 1}$-axes ratio: $\alpha = 0{\cdot}587 \simeq 0{\cdot}6 = \frac{3}{5}$. It seems that the (3, K, L, 0) and (0, K, L, 5) reflections are close enough in reciprocal space that the measurement of one intensity is increased by the tail of the corresponding reflection of the other subsystem. This effect is of course largest when the neighbouring reflection is a strong one, as was observed. The partial R factors for both subsystem reflection sets were thus increased with respect to their ideal value. As Pb is the strongest scatterer in this system, the largest effect was seen in the TiS_2 subsystem, thus explaining why the latter has the largest partial R factor. The common reflections do not include $H = 3$ or $M = 5$ reflections. They had the lowest partial R factor of 4·6%, indicative of a good fit.

* Lists of structure factors have been deposited with the British Library Document Supply Centre as Supplementary Publication No. SUP 53772 (24 pp.). Copies may be obtained through The Technical Editor, International Union of Crystallography, 5 Abbey Square, Chester CH1 2HU, England.

Table 5. *Crystallographic R factors for the final fits*

Partial R factors are defined using a subset of the reflections. The TiS_2 and PbS parts comprise the main reflections of the corresponding subsystem, excluding the common reflections (0, K, L, 0). The R factors are defined as $R_F = (\Sigma||F_{obs}| - |F_{calc}||)/(\Sigma|F_{obs}|)$ and $R_{F^2} = [\Sigma(|F_{obs}| - |F_{calc}|)^2 . \Sigma|F_{obs}|^2)^{1/2}$.

Reflection subset	Number of reflections	Basic structure R_F	Basic structure R_{F^2}	Modulated structure R_F	Modulated structure R_{F^2}
All	1449	0·076	0·072	0·069	0·064
TiS_2 part	331	0·130	0·137	0·088	0·097
PbS part	953	0·069	0·065	0·069	0·065
Common	165	0·048	0·046	0·048	0·046

Discussion

The projection of the structure along $\mathbf{a}_{\nu 2}$ and $\mathbf{a}_{\nu 1}$ is shown in Figs. 1 and 2, respectively. Comparing Fig. 2 with the corresponding projection for an orthorhombic misfit compound (Fig. 3), shows the different packing of the TS_2 (T = Ti, Nb) subsystem. As explained earlier, this different packing causes the deviation of α from 90° (Wiegers, Meetsma, van Smaalen *et al.*, 1990). The absence of the horizontal mirror plane is obvious from the S positions of TiS_2. It is noteworthy that the PbS atoms assume x_{22} values which compensate for $\alpha \neq 90°$. A pseudo **a** glide perpendicular to $\mathbf{a}^*_{\nu 3}$ was present for the basic structure of the PbS subsystem.

Interatomic distances within each subsystem are given in Table 8, for the case without modulation. The shortest Pb to S2 distance is between atoms at opposite sides of the PbS double layer. The average Pb to S2 distance (2·913 Å) is close to that observed in $(PbS)_{1.13}TaS_2$ (2·91 Å; Wulff, Meetsma, van Smaalen, Haange, de Boer & Wiegers, 1990) and to that in $(PbS)_{1.14}NbS_2$ (2·925 Å; Wiegers, Meetsma, Haange *et al.*, 1990). The two Ti to S1 distances are only slightly different, and are close to the corresponding distances in $(SnS)_{1.20}TiS_2$ (average distance is 2·425 Å) and 1*T*-TiS_2 (only a single distance of 2·428 Å; Chianelli *et al.*, 1975).

The incommensurability along the $\mathbf{a}_{\nu 1}$ axes is shown in Fig. 1. It appears that the shortest distances

Table 6. *Basic structure coordinates and temperature parameters* (Å^2) *as obtained by refinement of the modulated structure*

Coordinates refer to the subsystem lattice basis. Standard deviations in the last digits are given in parentheses. When these are not given, the corresponding parameters are fixed by symmetry. The temperature factor is defined in Table 3. For all atoms, U_{12} and U_{13} are zero as a consequence of the symmetry.

	ν	$x^0_{\nu 1}$	$x^0_{\nu 2}$	$x^0_{\nu 3}$	U_{11}	U_{22}	U_{33}	U_{23}
Ti	1	0·0	0·0	0·0	0·0135 (7)	0·0107 (6)	0·0133 (6)	0·0020 (5)
S1	1	0·5	0·1889 (3)	0·1222 (1)	0·0097 (6)	0·0083 (5)	0·0112 (5)	0·0026 (4)
Pb	2	0·25	0·0256 (1)	0·63638 (4)	0·0459 (3)	0·0318 (3)	0·0224 (2)	0·0032 (2)
S2	2	0·75	0·0184 (5)	0·5989 (3)	0·0500 (21)	0·0214 (15)	0·0210 (11)	0·0023 (11)

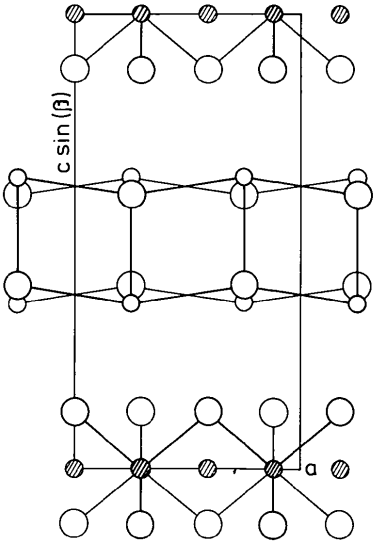

Fig. 1. Projection of the structure of $PbS_{1\cdot18}TiS_2$ along the $\mathbf{a}_{\nu 2}$ axes (**b** axes). Large circles denote S atoms, small circles denote Pb atoms and hatched circles denote Ti atoms. Thick lines represent atoms with $x_{\nu 2} \geq 0{\cdot}5$ and thin lines are used for atoms with $x_{\nu 2} \leq 0{\cdot}5$.

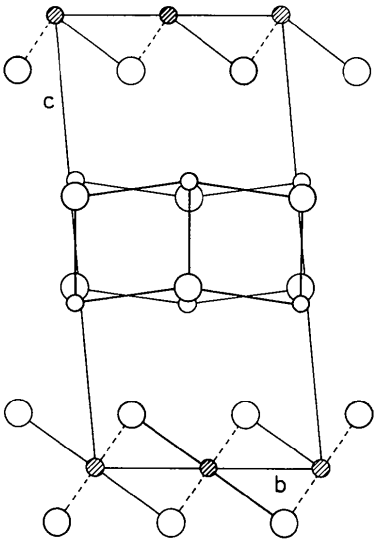

Fig. 2. Projection of the structure along the $\mathbf{a}_{\nu 1}$ axes. Large circles denote S atoms, small circles denote Pb atoms and hatched circles denote Ti atoms.

between the subsystems are between Pb ($\nu = 2$) and S1 ($\nu = 1$). Owing to the incommensurability, this distance varies with the position in the crystal. A comprehensive representation of this variation can be obtained by plotting the interatomic distance as a function of the fourth coordinate, t, in superspace (van Smaalen, 1991*b*; Onoda *et al.*, 1990).

The basic structure coordinates may already depend on t [equation (9)]. With the W^ν matrices given in (6), they are:

$$x_{1i} = n_{1i} + x^0_{1i}(j) \qquad i = 1, 2, 3 \qquad (22a)$$

$$x_{21} = n_{21} + x^0_{21}(j) - t \qquad (22b)$$

$$x_{2i} = n_{2i} + x^0_{2i}(j) \qquad i = 2, 3. \qquad (22c)$$

The values for $x^0_{\nu i}$ are given in Table 6. The arguments of the modulation functions are defined in (21). Their harmonic decomposition is given in (20), with parameters from Table 7. In each case these coordinates refer to the subsystem lattice basis Λ_ν. To be able to calculate atomic distances between atoms belonging to different subsystems, their coordinates have to be transformed to a single basis. Suitable transformation matrices are

$$(Z^\nu_3 + Z^\nu_d \sigma)^{-1} \qquad (23)$$

for $\nu = 1$, 2, respectively. Then, the transformed coordinates are with respect to the direct lattice basis belonging to the first three vectors of the set M

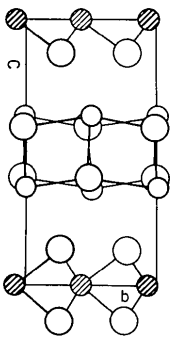

Fig. 3. Projection of the structure of the orthorhombic misfit compound $(SnS)_{1\cdot17}NbS_2$ along the $\mathbf{a}_{\nu 1}$ axes. Hatched circles are Nb atoms, small circles represent Sn atoms and large circles denote S atoms.

Table 7. *Modulation parameters for the best fit*

The amplitudes of the modulation function are defined in (20). For each atom, they refer to the subsystem basic vectors. For j = Ti, S1 ($\nu = 1$), the values correspond to B_{11}, A_{12} and A_{13}. For j = Pb, S2 ($\nu = 2$), the values correspond to A_{n1}, B_{n2} and B_{n3} (see Table 3, with $\tau_i = 0$). Standard deviations in the last digits are given in parentheses.

	A'_{n1}/B'_{n1}	A'_{n2}/B'_{n2}	A'_{n3}/B'_{n3}
First harmonic ($n = 1$)			
Ti	0·0	0·0004 (9)	0·0011 (5)
S1	−0·0003 (53)	−0·0011 (8)	−0·0005 (4)
Pb	−0·0008 (11)	−0·0108 (5)	−0·0004 (3)
S2	0·0013 (63)	0·0115 (26)	−0·0010 (19)
Second harmonic ($n = 2$)			
Pb	0·0005 (6)	0·0002 (7)	0·0007 (3)

Table 8. *Intrasubsystem distances* (Å) *for the average structure*

The superscript numbers refer to the curves in Figs. 8 and 9. With $x_i = x^0_{\nu i}$ corresponding to the coordinates in Table 6, the basic structure positions of the atoms are: Pb = $(x_1 + \frac{1}{2}, -x_2, 1-x_3)$, $S2^1 = (x_1, x_2, x_3)$, $S2^2 = (x_1 - \frac{1}{2}, -x_2, 1-x_3)$, $S2^3 = (x_1 + \frac{1}{2}, -x_2, 1-x_3)$, $S2^4 = (x_1, -x_2 - \frac{1}{2}, 1-x_3)$, $S2^5 = (x_1, -x_2 + \frac{1}{2}, 1-x_3)$, $S1 = (x_1, x_2, x_3)$, $Ti^1 = (x_1, x_2, x_3)$, $Ti^2 = (x_1 + 1, x_2, x_3)$ and $Ti^3 = (x_1 + \frac{1}{2}, x_2 + \frac{1}{2}, x_3)$.

Pb—$S2^1$	2·755 (3)	Pb—$S2^5$	2·975 (4)
Pb—$S2^{2,3}$	2·933 (1)	S1—$Ti^{1,2}$	2·431 (2)
Pb—$S2^4$	2·971 (4)	S1—Ti^3	2·428 (2)

[equation (1)]. The effect of the symmetry operators is given in (16). It is now easy to use (10) and (20)–(22) to calculate interatomic distances as a function of the fourth superspace coordinate t.

The interpretation of the distance *versus* t plots (Figs. 4–9) can be expressed as follows. For a pair of atoms, definite values for the coordinates in (22) and for the modulation function amplitudes [(10) and (20)], the distance can be calculated as a function of t. This results in a continuous curve. The distance at each value of t corresponds to the distance somewhere in the crystal. Generally, distances for nearby t values occur at widely separated positions in the crystal. Considering the distance of a single atom to all other atoms, or a selection of them, the collection of distances read off at a single t value corresponds to the distances between nearby atoms and the central atom placed somewhere in the crystal. Thus, considering all t values gives the variation of the coordination as a function of the position of the central atom in the crystal. The plots are given (Figs. 4–9) with Pb and S1 as central atoms.

First consider the distance between Pb ($\nu = 2$) and S1 ($\nu = 1$) in the basic structure. For one pair of atoms, with coordinates according to (22) and Table 6, the distance becomes infinite for t going to plus or minus infinity. This function is shown as one of the curves in Fig. 4. Obviously, it is not periodic. A periodic distance function can be obtained, when a single Pb atom is paired with all possible S1 atoms, and for each t the minimum distance is selected. As the incommensurability is only along $\mathbf{a}_{\nu 1}$, it is sufficient to consider all S1 atoms on a row parallel to $\mathbf{a}_{11}$ [n_{11} in (22) assumes all integer values]. A further complication is that there are two S atoms in the unit cell, of which either one may be closest to Pb. The first has coordinates as given in Table 6, the second is displaced by the centring translation $(\frac{1}{2}, -\frac{1}{2}, 0, -\frac{1}{2})$. The result is the plot given in Fig. 4. Curves marked A_1 and A_2 correspond to the two different S atoms. The shortest Pb to S1 distance, as a function of t, is obtained by starting in a minimum A_i and following the curve to a crossing point. Then the other curve is followed downwards to the other minimum A'_i.

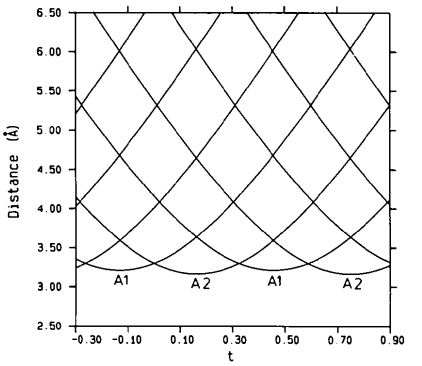

Fig. 4. Basic structure distances between Pb ($\nu = 2$) and S1 ($\nu = 1$) as a function of the fourth superspace coordinate t. The curves marked A_1 give the distance between (2, 1 0·0, 0, 1·0, 0·5) Pb and (E 1|n_{11}, 0, 0, 0) S1. The curves marked A_2 give the distance between (2, 1|0·0, 0, 1·0, 0·5) Pb and (E 1|n_{11} + 0·5, −0·5, 0, 0·5) S1. Equally marked curves correspond to different values for n_{11}, *i.e.* to different but translationally equivalent S atoms. Note that the symmetry operators refer to the standard superspace basis (G_s in Table 2).

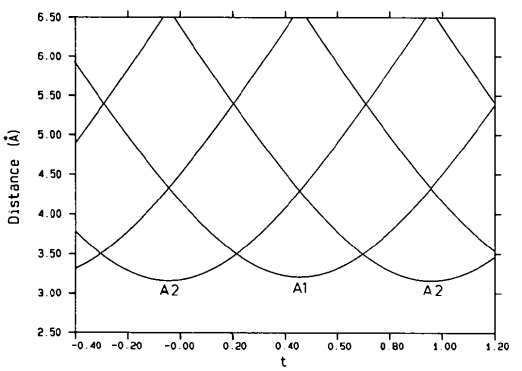

Fig. 5. Basic structure distances between S1 ($\nu = 1$) and Pb ($\nu = 2$) as a function of the fourth superspace coordinate t. The curves with a minimum marked A_1 correspond to the distance between (E 1|0, 0, 0, 0) S1 and (2, 1|0·0, 0, 1·0, n_{21} + 0·5) Pb. The curves marked A_2 define the distance between (E 1·0, 0, 0, 0) S1 and (2, 1|0·5, 0·5, 1·0, n_{21}) Pb. Equally marked curves correspond to different values for n_{21}. Note that the curves are equivalent to similarly marked curves in Fig. 4.

From Fig. 4, as well as from (21) and (22), it follows that the coordination of Pb by S1 results in a plot with a periodicity of $\alpha = 0{\cdot}5878$ in t. As follows from (21), this is the same periodicity as that of the PbS subsystem ($\nu = 2$). Alternatively, the Pb to S1 distances can be analyzed by considering the distance of S1 to all possible Pb atoms (n_{21} now assumes all integer values). This results in a plot which is periodic with periodicity 1 in t (Fig. 5). Again, this periodicity is the same as that of the subsystem of the central atom, now being subsystem 1. This means that the correlation between the effect of the modulation on the distances within substystem ν and the intrasubsystem distances could be studied by comparing the plot of the intrasubsystem distances *versus* t with either Fig. 4 ($\nu = 2$) or Fig. 5 ($\nu = 1$).

A more detailed representation of these distances is given in Figs. 6 and 7. Note that a curve marked A_i ($i = 1$, 2) in Fig. 7 is equivalent to the similarly marked curve in Fig. 6, but that the minimum may occur at different t values. Only a small variation in the minimum Pb to S1 distance was found; for the basic structure is was from 3·16 in A_2 to 3·30 Å in the crossing point B (Table 9). Figs. 6 and 7 also show the effect of the modulation on the interatomic distances. It was found that the modulation increases the shortest distance between the subsystems by 0·03 Å. The range of the shortest distance was decreased by the same amount: from 0·14 to 0·11 Å. This is a similar effect to that found in $(LaS)_{1{\cdot}14}NbS_2$, although the magnitude of the modulation is smaller for $(PbS)_{1{\cdot}18}TiS_2$.

The correlation between the coordinating S atoms also becomes clear from Fig. 6. A minimum in the shortest distance (points A) is accompanied by a maximum in the next shortest distance, of which

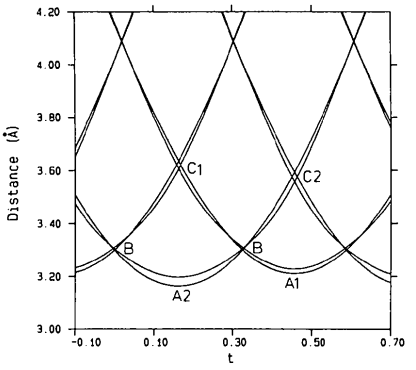

Fig. 6. Coordination of Pb ($\nu = 2$) by S1 ($\nu = 1$) as a function of the the fourth superspace coordinate t. Distances are calculated between the same atoms as given in Fig. 4. In the minima, the top curve defines the distance for the modulated structure.

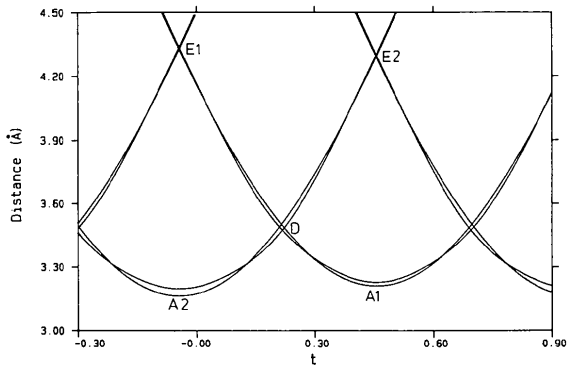

Fig. 7. Coordination of S1 ($\nu = 1$) by Pb ($\nu = 2$) as a function of the fourth superspace coordinate t. Distances are calculated between the same atoms as in Fig. 5. In the minima, the top curve represents the distance for the modulated structure.

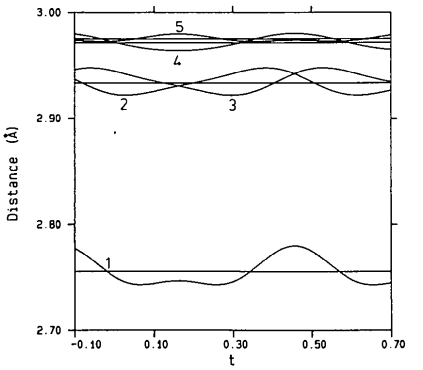

Fig. 8. Coordination of Pb ($\nu = 2$) by S2 of the same subsystem. The basic structure distances (horizontal lines) and the distances including the modulation are shown as a function of t. The curves correspond to the distance between (2_x 1|0, 0, 1·0, 0·5) Pb and the five following symmetry equivalents of S2: $S2^1$ = S2, $S2^2$ = (2_x 1|0, 0, 1·0, −0·5) S2, $S2^3$ = (2_x 1 0, 0, 1·0, 0·5) S2, $S2^4$ = (2_x 1 0·5, −0·5, 1·0, 0) S2 and $S2^5$ = (2_x 1 0·5, 0·5, 1·0, 0) S2. See Table 8 for the distances without the effect of the modulation.

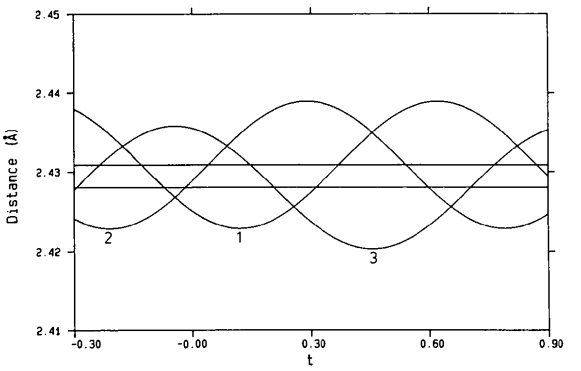

Fig. 9. Coordination of S1 ($\nu = 1$) by Ti atoms of the same subsystem. The basic structure distances (horizontal lines) and the distances including the modulation are shown as a function of t. The curves correspond to the distance between S1 and the following Ti atoms: Ti^1 = Ti, Ti^2 = (E 1|1·0, 0, 0, 0) Ti and Ti^3 = (E 1|0·5, 0·5, 0, 0·5) Ti. See Table 8 for the average structure distances.

there are then two equal ones. A maximum in the shortest distance (point *B*) gives a minimum in the next one, which is equal to the shortest distance. The distances in points *C* (Fig. 6) are 3·61 and 3·56 Å (Table 9). The difference between the corresponding shortest distances of 0·41 and 0·33 Å, respectively, makes it difficult to say whether this should be considered as a single or triple coordination of Pb by S1. For the coordination of S1 by Pb, it is immediately clear that the coordination varies between one (points A_i) and two (point *D*) (Fig. 7 and Table 9).

Fig. 8 shows the Pb to S2 distance. Again, a periodicity of $\alpha = 0{\cdot}5878$ in t was observed. The maximum variation was found for the Pb—S2 pair along $\mathbf{a}_{\nu 3}$ (curve 1), amounting to 0·06 Å, whereas the other distances varied less than 0·03 Å. This is small compared to the amplitudes of the modulation functions of Pb (0·06 Å) and S2 (0·07 Å), for which a maximum variation of $2 \times (0{\cdot}06 + 0{\cdot}07) = 0{\cdot}26$ Å can be expected. Apparently, the S2 atoms move in coherence with the Pb atoms, so as to minimize the variation. A correlation between the remaining variation in the distance of the Pb—S2 pair along $\mathbf{a}_{\nu 3}$ (curve 1) and the Pb to S1 distance (Fig. 6) could not be observed, contrary to the situation found for $(LaS)_{1.14}NbS_2$. An explanation might be that for the latter compound the La—S1 and La—S2 distances are of the same order, whereas for $(PbS)_{1.18}TiS_2$ the intersubsystem distances, Pb to S1, are 0·25 to 0·45 Å longer than the Pb to S2 distances. Other correlations between the intersubsystem and intrasubsystem distances of Pb to S cannot be discerned from either Fig. 6 or Fig. 8.

The distance of S1 to all possible Ti has periodicity 1 in t (Fig. 9). The variation is small, as the modulation amplitudes on both atoms are already small. A correlation between the S1 to Ti and S1 to Pb distances can be obtained as follows. From the information given in the figure captions, it can be inferred that curves 1 and 2 (Fig. 9) and the curve marked A_1 (Fig. 7) correspond to Ti and Pb atoms at the same side of S1 ($x_{\nu 2} \simeq 0$). The other curves correspond to metal atoms with $x_{\nu 2} \simeq 0{\cdot}5$. The minimum A_2 corresponds to Pb ($x_{22} = 0{\cdot}474$) closest to S1. In Fig. 9 curve 3 exhibits a maximum for this value of t. This means that Ti is at the same side of S1 as Pb and, with the same x_{11} as S1, it is at a maximum distance, in accordance with what one would expect from a simple repulsion model (Fig. 10*a*). Alternatively, when Pb ($x_{22} = -0{\cdot}024$) is at a minimum (A_1), the two Ti atoms at the same side of S1 as this Pb have a distance larger than average, but not a maximum. The reason is that the x_{11} coordinates for S1 and these two Ti atoms are no longer the same (Fig. 10*b*).

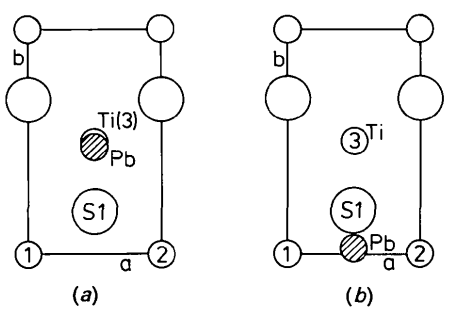

Fig. 10. Projection of a part of the structure onto the $(\mathbf{a}_{\nu 1}, \mathbf{a}_{\nu 2})$ plane. The TiS_2 unit cell is given, with Ti at $x_{13} = 0$ and S1 at $x_{13} = 0{\cdot}1221$, showing the coordination of S1 by three Ti atoms. (Not drawn are three S1 atoms at $x_{13} = -0{\cdot}1221$, which would complete the antiprismatic six-coordination of Ti.) The Pb atom ($x^0_{23} = 0{\cdot}362$) of the PbS subsystem closest to S1 is also given. (*a*) Corresponds to an A_2-type minimum separation, (*b*) is for an A_1-type distance. The numbers of the Ti atoms correspond to the same numbers as given in Fig. 9 and Table 8.

Table 9. *Interatomic distances between* Pb ($\nu = 2$) *and* S1 ($\nu = 1$)

The points refer to the atom pairs and t values as defined in Figs. 4–7.

Point	Basic structure distance (Å)	Modulated structure distance (Å)
A_1	3·21	3·23
A_2	3·16	3·20
B	3·30	3·31
C_1	3·64	3·61
C_2	3·59	3·56
D	3·50	3·47
E_1	4·32	4·34
E_2	4·29	4·30

Concluding remarks

In $(PbS)_{1.18}TiS_2$ the modulation mainly affects both atoms of the PbS subsystem. The largest displacements appear to be parallel to the layers, along the commensurate direction $\mathbf{a}_{\nu 2}$ (Table 4).

The coordination of Pb ($\nu = 2$) and S1 ($\nu = 1$) was studied by considering interatomic distances as a function of the fourth coordinate in superspace. In particular, the shortest distances from one atom to atoms of the other subsystem were calculated. It was shown that these functions have the periodicity of the subsystem to which the central atom belongs, allowing for an analysis of the correlation of intra- and intersubsystem distances. For Pb as the central atom, the variation in its distance to S1 was relatively small (Fig. 4), and of the same order as the variation in distances in ordinary modulated compounds. This gives a possible explanation for the relative stability of the inorganic misfit layer compounds. The effect of the modulation was found as a small increase of the shortest Pb to S1 distance.

The research of SvS has been made possible by financial support from the Royal Dutch Academy of Arts and Science (KNAW).

References

BOER, J. L. DE & DUISENBERG, J. M. (1984). *Acta Cryst.* A**40**, C-410.

CHIANELLI, R. R., SCANLON, J. C. & THOMPSON, A. H. (1975). *Mater. Res. Bull.* **10**, 1379–1382.

GOTOH, Y., GOTO, M., KAWAGUCHI, K., OOSAWA, Y. & ONODA, M. (1990). *Mater. Res. Bull.* **25**, 307–314.

JANNER, A. & JANSSEN, T. (1980). *Acta Cryst.* A**36**, 408–415.

KATO, K. (1990). *Acta Cryst.* B**46**, 39–44.

MAKOVICKY, E. & HYDE, B. G. (1981). *Struct. Bonding (Berlin)*, **46**, 101–170.

MEETSMA, A., WIEGERS, G. A., HAANGE, R. J. & DE BOER, J. L. (1989). *Acta Cryst.* A**45**, 285–291.

ONODA, M., KATO, K., GOTOH, Y. & OOSAWA, Y. (1990). *Acta Cryst.* B**46**, 487–492.

PETŘÍČEK, V. & COPPENS, P. (1988). *Acta Cryst.* A**44**, 235–239.

PETŘÍČEK, V., MALY, K., COPPENS, P., BU, X. CISAROVA, I. & FROST-JENSEN, A. (1991). *Acta Cryst.* A**47**, 210–216.

SMAALEN, S. VAN (1989). *J. Phys. Condens. Matter*, **1**, 2791–2800.

SMAALEN, S. VAN (1991*a*). *Phys. Rev. B.* In the press.

SMAALEN, S. VAN (1991*b*). *J. Phys. Condens. Matter*, **3**. In the press.

SPEK, A. L. (1982). *Computational Crystallography*, edited by D. SAYRE, p. 528. Oxford: Clarendon Press.

WIEGERS, G. A., MEETSMA, A., HAANGE, R. J., VAN SMAALEN, S., DE BOER, J. L., MEERSCHAUT, A., RABU, P. & ROUXEL, J. (1990). *Acta Cryst.* B**46**, 324–332.

WIEGERS, G. A., MEETSMA, A., VAN SMAALEN, S., HAANGE, R. J. & DE BOER, J. L. (1990). *Solid State Commun.* **75**, 689–692.

WIEGERS, G. A., MEETSMA, A., VAN SMAALEN, S., HAANGE, R. J., WULFF, J., ZEINSTRA, T., DE BOER, J. L., KUYPERS, S., VAN TENDELOO, G., VAN LANDUYT, J., AMELINCKX, S., MEERSCHAUT, A., RABU, P. & ROUXEL, J. (1989). *Solid State Commun.* **70**, 409–413.

WOLFF, P. M. DE, JANSSEN, T. & JANNER, A. (1981). *Acta Cryst.* A**37**, 625–636.

WULFF, J., MEETSMA, A., VAN SMAALEN, S., HAANGE, R. J., DE BOER, J. L. & WIEGERS, G. A. (1990). *J. Solid State Chem.* **84**, 118–129.

Acta Cryst. (1991). B**47**, 325–333

Caesium Substitution in the Titanate Hollandites $Ba_xCs_y(Ti^{3+}_{y+2x}Ti^{4+}_{8-2x-y})O_{16}$ from 5 to 400 K

BY ROBERT W. CHEARY

School of Physical Sciences, University of Technology Sydney, PO Box 123, *Broadway, New South Wales, Australia* 2007

(*Received* 30 *August* 1990; *accepted* 8 *January* 1991)

Abstract

Neutron powder diffraction data were collected for the titanate hollandites $Cs_{1\cdot36}Ti_8O_{16}$, $Cs_{0\cdot82}Ba_{0\cdot41}Ti_8O_{16}$ and $Cs_{0\cdot40}Ba_{0\cdot79}Ti_8O_{16}$ over the temperature range 5 to 400 K. Rietveld refinement was used to determine the tetragonal lattice parameters and the structural parameters of these compounds. The lattice parameters a and c increase with Cs concentration from $a = 10\cdot1688\,(2)$ and $c = 2\cdot9595\,(1)$ Å in $Cs_{0\cdot40}Ba_{0\cdot79}Ti_8O_{16}$ at 5 K to $a = 10\cdot2682\,(2)$ and $c = 2\cdot9643\,(1)$ Å in $Cs_{1\cdot36}Ti_8O_{16}$ at the same temperature. The expansion in these compounds is isotropic only in $Cs_{1\cdot36}Ti_8O_{16}$ with a linear-expansion coefficient of $\sim 8 \times 10^{-6}\,K^{-1}$ at 300 K. The presence of Cs is evident by the compression of the centres of the oxygen octahedral walls separating adjacent tunnels and by the enlargement of the tunnel cross-section. It is evident that the mean ⟨Ti—O⟩ bond length in the oxygen octahedra is influenced not only by the relative Ti^{3+}/Ti^{4+} concentration in the octahedra but also by the Cs in the tunnels. The oxygen box forming the cavity around each tunnel ion, Ba or Cs, is approximately 10% larger in $Cs_{1\cdot36}Ti_8O_{16}$ than in the pure Ba hollandite $Ba_{1\cdot07}Ti_8O_{16}$. All the tunnel ions are off-centred along the tunnel directions owing to the large size of Cs in relation to the intrinsically small tunnel cavities and the pairing of these ions in the tunnels. Positional disorder of all the ions is evident in the temperature factors, which possess a large temperature-independent component. The X-ray Debye temperature θ_M of each hollandite is in the range 420 to 460 K and the r.m.s. displacement of the tunnel ions along the tunnel axis arising from positional disorder is between 0·16 and 0·20 Å. In the context of hollandites being used as hosts for radioactive Cs in nuclear waste, an analysis is presented of the possibilty of Cs or Ba migration along the tunnels.

Introduction

A key aspect of the development of a solid wasteform for high-level nuclear waste is the immobilization of radioactive caesium. This element constitutes a major component of nuclear waste and is normally associated with extremely soluble compounds rather than chemically inert compounds. In the titanate wasteform known as SYNROC (Fielding & White, 1987) caesium is immobilized quite successfully with a leach resistance many orders of magni-

0108-7681/91/030325-09$03.00